Snapshots of Chemistry: Product Imaging of Molecular Reactions

PAUL L. HOUSTON

Department of Chemistry, Cornell University, Ithaca, New York 14853-1301

I. Introduction

Its unique fovea allows the human eye to perceive extremely fine detail, and it is perhaps because of this biological gift that humans rely more on what they can see than any other species. This "seeing is believing" trait has driven us to invent telescopes that view the most distant objects and microscopes that view the smallest. Using phenomena such as tunneling currents, interatomic forces, or near-field optics we are now able to "see" the structural consequences associated with chemical reactions. In this Account I will describe a different type of microscopy that allows us to see the dynamics of molecular reactions: to take snapshots of chemistry.

These snapshots measure the velocity distribution of a state-selected reaction product and tell us in what direction and how fast a product left the reaction center. There are many chemical problems for which knowledge of the velocity distribution of a selected product can provide details of the reaction mechanism. In a gas–surface interaction, for example, products leaving the surface with a cosine distribution relative to the surface normal can be presumed to have equilibrated with the surface before desorbing, whereas products that are more strongly directed toward a particular angle are likely to have experienced a repulsive release of energy. In photodissociation reactions, an anisotropic velocity distribution can be used to infer an upper limit on the dissociation lifetime, whereas an isotropic one indicates that the parent molecule is much longer lived than its rotational period. In crossed-beam reactions, scattering in the forward direction indicates a stripping mechanism, whereas scattering in the backward direction indicates a rebound mechanism. Symmetric forward–backward scattering is evidence for formation of a collision complex. Velocity distributions thus provide key details in interpreting the mechanism of a reaction.

Velocity snapshots are obtained using a technique similar to that used in a light microscope, where rays leaving different parts of the object are refracted by a lens to different angles and the amplification of the image to a macroscopic size is attained by letting the light travel a long distance relative to the size of the original image. Similarly, in velocity snapshots, products leaving the reaction center travel in different directions and with different speeds, and the amplification is achieved by allowing the particles to travel a long distance relative to their original spacing before they are detected. Fortunately, this process does not take a long time. Typical products travel out from their reaction center with velocities approaching 1 mm/μs, so that the observer need only be patient for on the order of 10 μs before the products have spread to a macroscopic size. The distribution of product positions after a measured time can be used to determine their velocity distribution. With modern position sensitive detectors and multiarray digital cameras, all positions can be determined simultaneously, allowing a tremendous enhancement in signal-to-noise.

The first snapshot we obtained[1] for a molecular reaction is shown in Figure 1. Understanding it will lead us to a deeper appreciation for the method and show the power of the technique. The reaction we studied is the photodissociation of methyl iodide, and the product that is imaged is the methyl radical in low rotational levels of its lowest vibrational level. The experiment involves taking a beam of methyl iodide molecules and crossing it with a dissociation laser operating at 266 nm. At this wavelength, nearly all of the iodine atoms created in the dissociation are in their first electronically excited state, the $^2P_{1/2}$ state. The energy deposited into the methyl iodide by the photon thus goes (1) to break the C–I bond, (2) to excite the iodine product electronically, and (3) to provide the recoil velocity between the iodine atom and the detected methyl radical. Because the energies of the photon and of processes 1 and 2 are all sharply defined, the energy available for process 3 must also be sharp, and thus the detected methyl radicals should be traveling outward from the methyl iodide center of mass with nearly a single speed. We can imagine them as being located, though not necessarily uniformly, on the surface of a sphere whose radius expands in time with the methyl velocity. The snapshot detects the image made when the methyl radicals on this sphere fly into a screen. The snapshot is thus a two-dimensional projection of the three-dimensional velocity distribution. Note that a single sphere is observed. Had some of the methyl radicals been produced in coincidence with the ground state of iodine ($^2P_{3/2}$), we would have expeced to see in addition the projection of a larger sphere superimposed on the image. The absence of the larger sphere tells us that the methyl radicals are produced almost exclusively in coincidence with the spin–orbit excited state, I($^2P_{1/2}$).

Paul L. Houston received his B.S. degree from Yale University in 1969 and his Ph.D. from the Massachusetts Institute of Technology in 1973. After spending two years as a postdoctoral research associate at the University of California, Berkeley, he moved to Cornell University, where he is now a professor of chemistry. He has been a visiting scientist at the Max Planck Institute for Quantum Optics and the Institute for Molecular Science and a visiting professor at Columbia University. His research interests center on applications of lasers to chemical problems, particularly photodissociation, energy transfer, and gas–surface interactions. He is a senior editor of the *Journal of Physical Chemistry.*

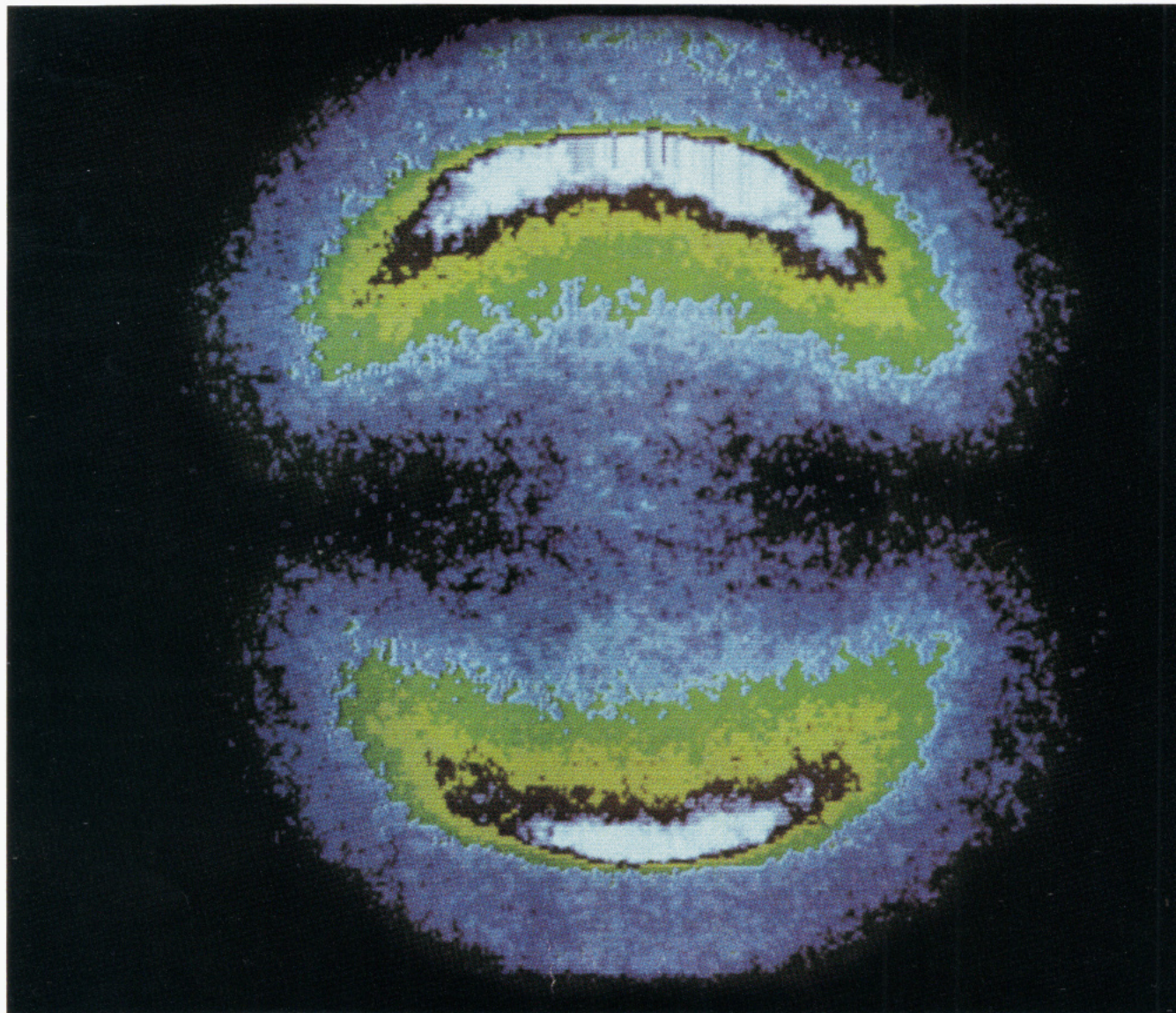(1) Chandler, D. W.; Houston, P. L. *J. Chem. Phys.* **1987,** *87,* 1445–1447.

Figure 1. Velocity snapshot of the methyl radical in its lowest vibrational level following photodissociation of methyl iodide at 266 nm. The polarization direction of the dissociation laser is along the north–south axis of the image.

It is obvious from Figure 1 that the methyl velocities are not uniformly distributed on the sphere, since their two-dimensional projection has much more intensity at the north and south poles than around the equator. The reason for this anisotropy involves the linear polarization of the dissociation laser and the location of the transition dipole moment in the methyl iodide; the former is aligned in this experiment along the north–south axis of the figure, while the latter is located along the C–I bond. Because the methyl iodide will absorb with higher probability if its transition dipole is aligned along the oscillating electric field of the dissociating light, the excited methyl iodide molecules will preferentially have their C–I bonds located along the north–south axis. If the methyl iodides then dissociate more rapidly than they rotate, we might expect the methyl and iodide fragments to fly out along the breaking bond, toward the north or south pole. Indeed, this is exactly what is observed.

Before moving to other examples let us consider how the products are state-selected and detected. In the snapshot technique, the products are actually detected as ions, and they are ionized by using a second laser to induce a process known as $n + m$ resonant multiphoton ionization. In this scheme, products in a spectroscopically selected vibrational and rotational state are first excited to an intermediate electronic state by n laser photons and then further excited by m more photons to the ionization limit. The methyl ionization used in Figure 1, for example, is a $2 + 1$ multiphoton process. Because the ejected electron has such small mass compared to the product, the velocity distribution of the product ions is nearly identical to the velocity distribution of the product neutrals. The advantages of the ionization are (1) that only products in the spectroscopically selected state are ionized and detected and (2) that the detection of ions is much easier than that of neutrals. In our case, the ions are detected by a pair of microchannel plates, essentially ceramic disks with close-packed, 10-μm-diameter channels. The inner walls of the channels are coated with a material that emits secondary electrons when struck by an accelerated ion. The electrons are then amplified (by a factor of about 10^6–10^7) as they travel up the channels and then accelerated to a phosphorescent screen. In the original apparatus,[1] light from the

phosphorescent screen was detected by eye, but subsequent improvements have used both a regular camera and a digitizing charge injection device (CID) camera.

Under most conditions, the two-dimensional projection can be used to reconstruct the full three-dimensional velocity distribution because the latter has cylindrical symmetry. Consider, for example, the photodissociation case. Methyl iodide molecules with their C−I bond at a particular angle to the polarization direction of the dissociation laser will have equal probabilities for being dissociated regardless of azimuthal angle; that is, there will be cylindrical symmetry of the C−I bond angles and thus the methyl velocities about the polarization direction. Assuming that the ionization scheme does not depend on azimuthal angle,[2] the cylindrical symmetry will extend to the detected ions. If the projection is then made in a direction perpendicular to the cylindrical axis, as is the case for Figure 1, then one snapshot is sufficient to recover the three-dimensional information. A logical explanation for this assertion is provided by mathematics. If we have three dimensions—say r, θ, and ϕ—but the distribution does not depend on one of them (ϕ), then the three-dimensional object really contains only two dimensions of information. Since the two-dimensional projection also contains two dimensions of information, no information is lost in making the projection. In fact, a standard technique, called the inverse Abel transformation, can be used to recover the three-dimensional object from its two-dimensional projection.[3,4] An explanation for this assertion at a more intuitive level can be grasped by imagining a side view of, say, two nested glass objects, each with cylindrical symmetry: for example, a soda bottle inside a beaker. What we see from a distance is close to a two-dimensional projection of the light absorption caused by this cylindrical object. For every line across the projection, we see discontinuities of absorption where the beaker starts and ends, and further discontinuities where the soda bottle starts and ends. Knowing that both objects have cylindrical symmetry allows us easily to reconstruct in our mind the three-dimensional image that gave rise to the projection we see. The Abel transform simply quantifies this process by looking at every line across the projection and determining the cylindrical objects that gave rise to the intensity distribution along this line.

The remaining sections provide two examples of how velocity snapshots can be used to interpret chemical reactions. In section II we will use these images to learn the details of crossed-beam reactions. In section III, we will then return to photodissociation processes and see how the speed distribution for the O atom from the dissociation of ozone can be used to help resolve a long-standing problem in atmospheric chemistry. The Account ends with some general conclusions and predictions for the future.

(2) For an example of how even more can be learned by using a polarized ionization source to breaking the cylindrical symmetry, see Suits et al., in which it is shown that snapshots can be used to measure the alignment of chemical products: Suits, A. G.; Miller, R. L.; Bontuyan, L. S.; Houston, P. L. *J. Chem. Soc., Faraday Trans.* **1993**, *89*, 1443–1447.

(3) Castleman, K. R. *Digital Image Processing*; Prentice Hall: Englewood Cliffs, NJ, 1979.

(4) Schepp, L. A.; Logan, B. F. *IEEE Trans. Nucl. Sci.* **1974**, *NS-21*, 21.

II. Crossed Molecular Beam Reactions

An example of the power of the velocity-imaging technique is provided by a study of the rotational excitation of NO molecules following their collision with argon atoms.[5] What we would like to determine is the scattering distribution. Are the NO products forward or backward scattered relative to their initial velocity, and how does the scattering distribution depend on the rotational level of NO produced? What makes this a good illustration of the snapshot technique is not that rotational excitation of NO by argon is such an important chemical process, but rather that the measurement is very difficult by other techniques. The energy separation between different rotational levels of the product corresponds to only a few wavenumbers, so that differentiation between the final states, for example by the time-of-flight techniques used in conventional crossed-beam scattering machines, would be nearly impossible. To observe the scattering distribution of state-selected products, we need some way spectroscopically to label the products of interest. Fortunately, the multiphoton ionization step provides this labeling automatically in our snapshots.

A complication in understanding crossed molecular beam reactions is the conversion between the laboratory frame, defined by the directions of the two molecular beams, and the center-of-mass frame, defined by the relative velocity between the colliding reactant pair. A side benefit of the snapshot technique is that it allows us to "see" what is happening. Figure 2 shows what is happening schematically, while Figure 3a shows an actual image of the two molecular beams. A beam formed from an expansion of a few percent NO in a helium carrier gas propagates from right to left in the figures. Because the expansion cools the beam, most of the NO is in its lowest rotational level, $J = 0.5$.[6] The molecular beam is observed by being illuminated with a pulsed laser tuned to ionize NO in this lowest rotational level. The argon beam travels from top to bottom in the figure, and it is made visible by introduction of a little NO into the beam and illumination with a second pulsed laser beam tuned similarly. In addition to the two molecular beams, three spots are visible in Figure 3a and identified in Figure 2. One spot occurs where the two beams intersect. A second spot, which I will call the "NO spot", occurs to the left of this intersection and is caused by molecules in the NO beam that absorbed light at the intersection point from the laser aimed along the argon beam. In the time it takes for these NO molecules to travel from the intersection point to a detector located above the plane of the beams, they also travel left to the new "NO spot". The distance traveled and the time measured between the ionization laser pulse and the arrival of the ions at the detector determine the initial velocity of the NO beam. Furthermore, the height and width of the NO spot can be used to determine the dispersion and width of the NO molecular beam, quantities necessary for an accurate interpretation of the data. In a similar

(5) Bontuyan, L. S.; Suits, A. G.; Houston, P. L.; Whitaker, B. J. *J. Phys. Chem.* **1993**, *97*, 6342–6350.

(6) The levels of NO have half-integral labels because the total rotational angular momentum consists of the vector sum of the integral end-over-end tumbling angular momentum and the half-integral spin angular momentum of the unpaired electron.

456 *Acc. Chem. Res., Vol. 28, No. 11, 1995*

Houston

way, NO in the argon beam absorbed light at the intersection point from the laser illuminating the NO beam, and this NO traveled downward with the argon velocity to the third spot on the figure, which I will call the "argon spot". The line superimposed on the figure between the argon spot and the NO spot provides a measure of the relative velocity between the NO and argon.

Now consider an individual argon atom entering the diagram from the top and colliding with an individual NO molecule entering the diagram from the right. The center of mass of this Ar−NO system is always between the pair and a bit closer to the argon than the NO due to its greater mass. As the pair collides, the center of mass moves from the upper right of the figure through the intersection point toward the lower left. At the time when, in the absence of a collision, the NO would be at the NO spot and the argon at the argon spot, the center of mass of the system would lie on the relative velocity line between these two spots and somewhat closer to the argon spot. In this center-of-mass frame, the NO and Ar are moving with the directions indicated in Figure 2.

Consider NO molecules that do not change their original speed and that are undeflected by the collision. These are, by definition, forward scattered and would be detected near the "NO spot". In contrast, if an NO molecule collided with an argon and bounced exactly backward, it would be detected 180° from the NO spot, *i.e.*, at a point near the argon spot but a bit farther away than this from the center of mass. Of course exact forward or backward scattering is an extreme limit, and most scattering will occur at other angles. The circle superimposed on the image represents the size of a sphere, the so-called "Newton sphere", on which the NO products would be found if their speed were not changed by the collision.

Figure 3b−f shows the images obtained for Ar−NO collisions, where the final rotational state of the NO has been selected spectroscopically by the ionization step. Product molecules in $J = 7.5$ are scattered nearly in the forward direction and arrive near the NO spot. Products in $J = 11.5$ are almost forward scattered, but they arrive preferentially in a small range of angles near about 30° from the forward direction. Products in $J = 14.5$ and 18.5 show angular peaks that are progressively more in a sideward direction, while products in $J = 24.5$ are nearly backward scattered. Note in addition that there seem to be two peaks for the $J = 18.5$ distribution.

The explanation for many of these features follows from the classical mechanics of hard spheres (argon atoms) hitting hard ellipsoids (NO molecules).[7,8] The peaks in the angular distribution are called "rotational rainbows", and they share similarities with their celestial namesake in that many angular orientations and impact parameters contribute to scattering over a small range of angles. Even the simple hard-ellipse collision model predicts rotational rainbows, and it is easy to see why the rainbow angle shifts to larger angles with increasing J. Consider first an NO molecule that has just a glancing collision with an argon. Because very little momentum is exchanged in the collision, the NO is not expected to change its
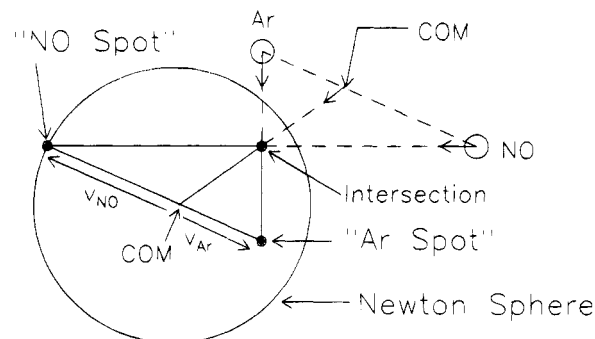
(7) Bosanac, S. *Phys. Rev. A* **1980**, *22*, 2617.
(8) Bosanac, S.; Buck, U. *Chem. Phys. Lett.* **1981**, *81*, 315.

Figure 2. Schematic drawing of the image shown in Figure 3a, identifying the center of mass of the Ar−NO system before and after the collision and the three spots mentioned in the text.

rotational level from $J = 0.5$ to a very much higher level, and because the collision is glancing, the NO final velocity is nearly the same as its initial velocity. Thus, we find that forward scattering is dominant for low rotational levels of the products. To produce high rotational levels, the collision must transfer substantial momentum from translational into angular degrees of freedom, and it can do this only if the collision occurs at close quarters. However, these low-impact-parameter collisions are also expected to result in large scattering angles, since now the NO and argon must meet nearly head-on. Thus, backward scattering is dominated by high rotational levels of the NO product. Between these limits, the rotational rainbow predicted by hard sphere−ellipsoid collisions simply moves continuously from the forward direction to the backward direction. The way in which the angle of the rainbow varies with J provides valuable information about the interaction potential between Ar and NO. If we represent the repulsive wall of the NO by a hard ellipsoid, the difference in distance between the semimajor and semiminor axes can be determined from the data to be about 0.30 Å.

But why are there two rainbows for $J = 18.5$? In fact, there are two rainbow angles for all final rotational levels, but they are most easily resolved when the scattering is in the sideward direction. The reason for the double rainbow is that NO rotates about its center of mass rather than about the center of the ellipse that we have used to approximate its repulsive wall. Scattering can occur from either end of the NO molecule, and the two ends are rotating about the center of mass at slightly different radii. By carefully measuring the angular difference between the two rainbows for $J = 18.5$ and comparing with the hard-ellipse model, we can determine that the center of the repulsive ellipse is shifted about 0.05 Å from the NO center of mass.

What I have tried to demonstrate in this example is that snapshots of the velocity distribution produced in crossed-beam interactions can provide useful details about the mechanism of a chemical process. The principal scientific advantages of the technique are that one can determine the scattering distribution for any state that can be selected spectroscopically and that scattering to all angles can be collected simultaneously. But there is an appealing aesthetic advantage as well: the snapshot allows us to actually "see" what happens.
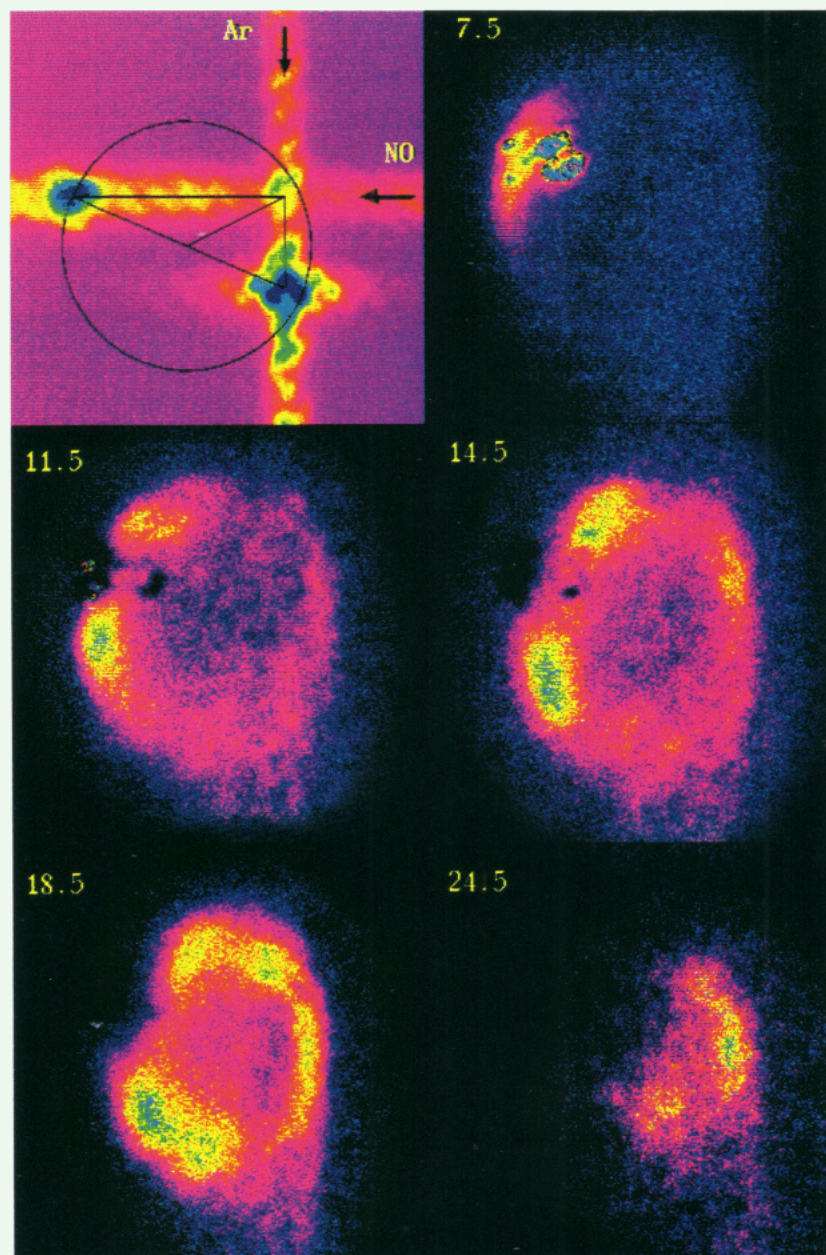
Figure 3. (a, top left) Image of argon and NO molecular beams showing the beams themselves as well as three spots: the spot representing intersection of the molecular beams, a spot to the left representing the initial NO velocity, and a spot below the intersection representing the argon velocity. Superimposed on the image are lines representing the relative velocity and the center-of-mass velocity. The circle represents the sphere on which NO products would be found if their speed were not changed by the collision. (b−f) Images of the NO product of the collision of NO with argon for various final rotational levels of NO: b, $J = 7.5$; c, $J = 11.5$; d, $J = 14.5$; e, $J = 18.5$; f, $J = 24.5$. As the final rotational level increases, the scattering distribution shifts from forward to sideward to backward.

III. The Photodissociation Dynamics of Ozone and the "Ozone Deficit" Problem

It often occurs that, when new techniques are applied to old problems, surprising results are obtained. The photodissociation of ozone in the near ultraviolet region of the spectrum produces two sets of products. The major product channel, accounting for about 90% of the yield, gives electronically excited products $O(^1D)$ + $O_2(^1\Delta_g)$, while the minor channel, accounting for the other 10%, gives ground-state products $O(^3P)$ + $O_2(^3\Sigma_g^-)$. In this last example[9] we will turn to the dissociation of ozone and describe a new observation made possible by the snapshot technique that may explain a long-standing question concerning the concentration of ozone in the stratosphere.

The new observation is shown in Figure 4, which displays the symmetrized two-dimensional projection of the velocity distribution for the $O(^3P_2)$ atomic product of the dissociation of ozone at 226 nm. It is not surprising to find that most of the atomic fragments fly to the north or south pole in this figure, since that is the direction of polarization of the dissociation laser and since the ozone transition dipole moment is nearly along the breaking bond. However, it is surprising to find that the O atom speeds cluster around two values rather than displaying a single peak. While some fragments have high enough speeds to reach the top and bottom lobes on the outer limits

(9) Miller, R. L.; Suits, A. G.; Houston, P. L.; Toumi, R.; Mack, J. A.; Wodtke, A. M. *Science* **1994**, *265*, 1831−1838.
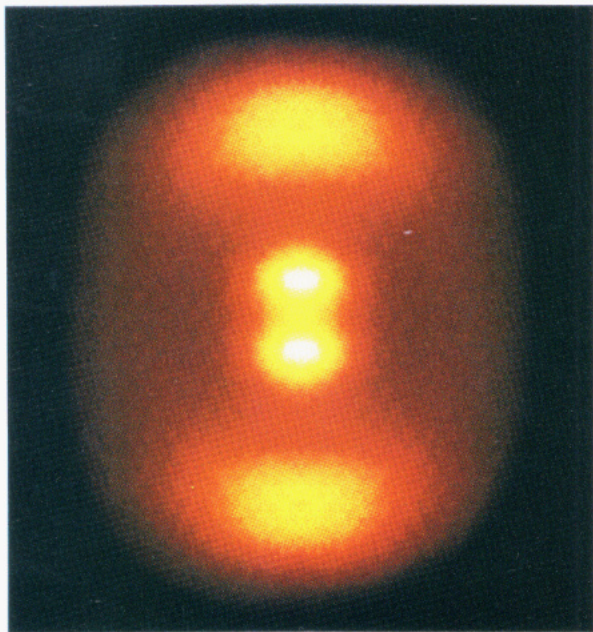
Figure 4. Symmetrized image of the two-dimensional projection of the velocity distribution of $O(^3P_2)$ created in the 226-nm dissociation of ozone. The dissociation light was polarized in the vertical direction for this image.

of the image, others move much more slowly and are grouped in the two lobes near the center. These slower fragments were completely unexpected.

Careful analysis of images like that in Figure 4 yields the distribution of translational energy for the photodissociation shown in Figure 5. While most dissociations produce O and O_2 fragments that have translational energies of about 2 eV, some dissociations produce translational energies of only 0.2 eV. Conservation of energy allows us to deduce a surprising result. We know how much energy the 226-nm photon deposits into the O_3 (5.49 eV). A known amount of this energy goes to break the O_2–O bond (1.05 eV), and a measured amount of the energy appears in relative translation, as shown on the bottom axis of the figure. The remaining amount has to appear somewhere, and the only possible repository for this energy is in the internal degrees of freedom of the O_2 product. Thus, as we read increasing translational energy from left to right on the lower abscissa of Figure 5, we can also read decreasing O_2 internal energy, as shown along the top abscissa. The dissociations that produce the peak in the translational energy distribution near 0.2 eV must produce a peak in the internal energy distribution of the O_2 near 4.2 eV. The only likely place for this energy to be is in the vibrational degrees of freedom. The comb on the figure identifies the energies associated with various vibrational levels; the low translational energy dissociations produce O_2 with 27 quanta of vibrational energy, almost enough vibrational energy to dissociate the molecule! The assertion that this energy is in vibration has been confirmed by measuring parts of the O_2 vibrational distribution by a laser-induced fluorescence technique. The points with error bars on the figure give the results of this measurement and are in agreement with the interpretation that the O_2 internal energy is vibrational. These very highly vibrationally excited O_2 product molecules had not been previously observed in the dissociation of ozone.

It is important to note that the newly observed dissociation products are, in fact, a very minor dissociation channel. The yield of the $O(^3P) + O_2(^3\Sigma_g^-)$ product channel is only about 10% of the total yield, and the highly vibrationally excited peak in the distribution of Figure 5 is only about 10% of this minor channel. The new peak in the distribution would not have been found at all if it were not for the state-selective nature of the detection process used to obtain the snapshot.

Because of the small yield, it does not at first seem likely that the new peak in the distribution can have much consequence in influencing the concentration of ozone in the stratosphere. Furthermore, the results are for the dissociation of ozone at 226 nm, a spectral region where the combination of absorption coefficient and solar flux contributes less to the total ozone dissociation in the stratosphere than at longer wavelengths. We were thus surprised to discover that the new peak in the distribution might explain a long-standing discrepancy between the predicted and the measured ozone concentration in the upper stratosphere.

This problem, known as the "ozone deficit", really refers to a deficit in our understanding rather than to missing ozone in the stratosphere. The concentration of ozone in the stratosphere is indeed decreasing, but atmospheric chemists understand that the decrease is due to increasing amounts of radicals like chlorine atoms that catalyze the conversion of ozone to oxygen. What they do not understand is why their calculations of the concentration of stratospheric ozone always predict about 10–20% less ozone than is observed in balloon or satellite flights. Despite its small yield, the newly observed peak in Figure 5 appears to offer an explanation.

The explanation has three parts. One is the conjecture, based on indirect kinetic measurements, that the highly vibrationally excited O_2 produced in the dissociation can react with unexcited O_2 to give O_3 + O.[10] A second is the realization that the dissociation and reaction provide an *autocatalytic* mechanism for the production of ozone. One ozone molecule is photodissociated, producing an O atom and a vibrationally excited O_2. The latter species reacts with O_2 to give O + O_3, and under stratospheric conditions each O atom recombines with O_2 to give O_3. Thus, each photodissociation by this route consumes one ozone molecule but produces three. The final and most important part of the explanation is that each ozone molecule in the stratosphere is dissociated several hundred times during its chemical lifetime, so that the autocatalytic reaction is amplified by a very large factor. In fact, when the new ozone dissociation mechanism is included in global stratospheric ozone calculations, a 10% increase in ozone concentration over that predicted without the new mechanism is found for an altitude of 42 km: the ozone deficit completely disappears at the altitude where the absolute discrepancy is largest. The calculation is not so successful at other altitudes, but it naively assumes that the yield of the newly discovered channel is constant as a function of dissociation wavelength in the energetically permitted spectral region. Measure-

(10) Rogaski, C. A.; Price, J. M.; Mack, J. A.; Wodtke, A. M. *Geophys. Res. Lett.* **1993**, *20*, 2885.
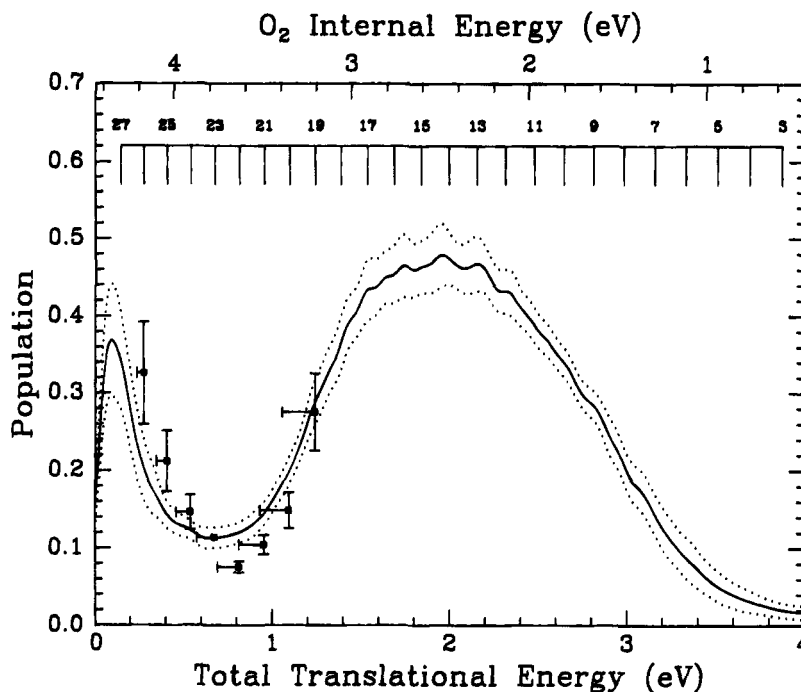
Figure 5. The average translational distribution for the dissociation of O_3 to $O(^3P) + O_2(^3\Sigma_g^-)$ at 226 nm. The bottom abscissa gives the translational energy, and the top abscissa gives the corresponding O_2 internal energy. The vibrational levels of O_2 are indicated from 3 to 27 on the comb. The smooth line gives the energy distribution derived from the photofragment imaging experiment, and the dotted lines give the $\pm 1\sigma$ error limits. The points with error bars give the energy distribution derived from a laser-induced fluorescence experiment. Reprinted with permission from ref 9. Copyright 1994 American Association for the Advancement of Science.

ments of the wavelength dependence of the yield of vibrationally excited O_2 and direct observation that the reaction of this species with unexcited O_2 occurs to give $O_3 + O$ are needed before we can see if the new mechanism accounts completely for the deficit.

IV. Conclusions and Future Directions

We have seen examples of how snapshots of velocity distributions can provide detailed information about chemical reactions. We can learn, for example, how the scattering distribution in a crossed-beam reaction depends on the internal energy of the reaction product, and from such information we can deduce important parameters of the interaction potential. In the case of photodissociation dynamics, we can determine if the scattering is anisotropic, indicating an excited-state lifetime short compared to rotation, or isotropic, indicating a long-lived excited state. The high selectivity of the new technique allows us to focus on specific reaction channels, even those which while having only minor yield might have important practical consequences. The principal advantages of the new technique are that the data for scattering in all directions is collected at once and that this data can be obtained for products in selected internal energy states.

There are, of course, some limitations. In the current version we need to be able to ionize the product species in a state-selected fashion. Modern lasers make more and more systems amenable to this technique, but there are some products that will always be difficult to ionize. Fortunately, similar imaging techniques using, for example, laser-induced fluorescence are now extending the possibilities. The angular and velocity resolution of our current snapshots are still not competitive with conventional, albeit large, molecular beam machines, principally because the scattering distance that can be achieved in these

machines is much greater than the diameter of current microchannel plate detectors. However, these detectors are now being fabricated with larger and larger areas, so that many problems that are just beyond our reach now should soon become accessible.

It is particularly encouraging that imaging techniques are spreading to many other fields of physical chemistry. In addition to its use in photodissociation and crossed molecular beam studies, imaging has recently been adapted to study scattering from surfaces.[11-13] A recent workshop[14] outlined a wide variety of imaging applications, including photodissociation dynamics, imaging of metastable species, ion processes, free radical photodissociation, and molecular structure determination. It thus appears that imaging techniques will pervade many areas of physical chemistry.

Although the product-imaging technique is now in use by many groups, there remain several features that might still be exploited to learn new chemistry. For example, one might mask the detection screen so that only those products that are both in the spectroscopically selected state and possessing a selected velocity are detected. For selected velocities near zero, it should be possible to achieve a velocity resolution corresponding to a few wavenumbers. What chemical problems could be solved by an ability to detect, for example, zero-kinetic-energy photofragments in selected internal energy levels?

Space limitations in this Account have not permitted

(11) Corr, D.; Jacobs, D. C. *Rev. Sci. Instrum.* **1992**, *63*, 1969–1972.
(12) Morris, J. R.; Martin, J. S.; Greeley, J. N.; Jacobs, D. C. *Surf. Sci.* **1995**, *330*, 323–336.
(13) Menges, M.; Baumeister, B.; Al-Shamery, K.; Freund, H.-J.; Fischer, C.; Andresen, P. *Surf. Sci.* **1994**, *316*, 103.
(14) Workshop on Imaging Methods in Molecular Structure and Dynamics, Neve Ilan, Israel, June 13–16, 1994; D. Zajfman and G. C. McBane, organizers.

more than a reference,[15] but it is also possible to determine the alignment of products using the snapshot technique. If we could couple this ability with newly developed methods for aligning or orienting state-selected reactants, we should be able, in favorable cases, to achieve the long-sought goal of "completely" describing a chemical reaction. The desired description is generally obscured by the inherent averaging over impact parameter and angle of attack, even when we specify the initial velocities. Measurement of the angular distribution of the products by the snapshot technique helps us to unravel the former type of averaging, while the correlation between initial and final alignments can help us to unravel the latter. Thus, it may soon be possible to obtain the maximum information from a chemical reaction.

(15) Suits, A. G.; Miller, R. L.; Bontuyan, L. S.; Houston, P. L. *J. Chem. Soc., Faraday Trans. 2* **1993**, *89*, 1443−1447.

New chemistry aside, one of the biggest advantages of the snapshot technique is that it allows us to "see" the dynamics of the reaction, and perhaps even to believe that it has happened.

AR950130Q